Monte Carlo study of the ordering of the weakly anisotropic Heisenberg spin glass in magnetic fields

Daisuke Imagawa and Hikaru Kawamura
Department of Earth and Space Science, Faculty of Science, Osaka University, Toyonaka 560-0043, Japan
(Dated: February 2, 2008)

The ordering of the three-dimensional Heisenberg spin glass with the weak random anisotropy in magnetic fields is studied by extensive equilibrium Monte Carlo simulations. Both the spin and the chirality are monitored. We find strong numerical evidence that a replica symmetry breaking transition occurs in the chiral sector, which accompanies the simultaneous spin-glass order. Despite the similarity in the global symmetry, the ordering behavior of the weakly anisotropic Heisenberg spin glass differs significantly from that of the strongly anisotropic Ising spin glass. The obtained phase diagram in the temperature - magnetic field plane is similar to the experimental phase diagram. Our results highlight the importance of the chirality in the spin-glass ordering of the Heisenberg-like spin glass, and support the spin-chirality decoupling-recoupling scenario of spin-glass transitions.

I. INTRODUCTION

Spin glasses (SGs) are random magnets where ferromagnetic and anti-ferromagnetic exchange interactions coexist and compete.[1] Experimentally, it is now well established that SG magnets in zero field exhibit a thermodynamic second-order phase transition at a nonzero temperature into the thermodynamic SG phase. By contrast, whether SG magnets exhibit a thermodynamic phase transition in applied magnetic fields has been a long-standing, yet unsolved issue. This issue is closely related to the fundamental question of whether the SG ordered state in zero field accompanies an ergodicity breaking not directly related to the global symmetry of the Hamiltonian, *i.e.*, the replica symmetry breaking (RSB).

The experimental evidence of an in-field transition of SG remains to be obscure. For the strongly anisotropic Ising-like SG, $Fe_{0.5}Mn_{0.5}TiO_3$, the non-existence of an in-field SG transition was reported in Ref.[2]. Meanwhile, many of real SG materials are more or less Heisenberg-like rather than Ising-like in the sense that the magnetic anisotropy is considerably weaker than the isotropic exchange interaction.[1] Recent experiments on such weakly anisotropic Heisenberg-like SGs suggested the occurrence of an in-field SG transition,[3,4] in apparent contrast to Ref.[2]. Setting aside the question of the strict nature of the apparent SG "transition" observed experimentally in applied fields, it has been known that the "transition line" between the paramagnetic and the SG phases is similar to the one obtained for the mean-field Sherrington-Kirkpatrick (SK) model:[5] Namely, in the weak field regime, the in-field transition temperature, $T_g(H)$, is rapidly suppressed with increasing the field intensity H, as $H \propto |1 - T_g(H)/T_g(0)|^{3/2}$ (de Almeida-Thouless (AT) line[6]), while in the high field regime, $T_g(H)$ stays rather robust against H, behaving as $H \propto |1 - T_g(H)/T_g(0)|^{1/2}$ (Gabay-Toulouse (GT) line[7]). However, the reason why the mean-field results have given such a good description of the phase boundary, including the values of the critical exponents describing the phase boundary, has remained to be a mystery.

On the theoretical side, most of numerical studies on the finite-ranged SG models in three dimensions (3D) have focused on the properties of the Ising SG.[1] Since no global symmetry exists in the Ising SG under magnetic fields, an in-field transition, if any, should be a pure RSB transition. Unfortunately, numerical simulations on the Ising SG have been unable to give a definitive answer concerning the existence of a thermodynamic SG transition in magnetic fields.[8,9,10,11,12,13,14,15,16,17,18]

For the isotropic 3D Heisenberg SG in zero field, it has been believed for years that the SG transition occurs only at zero temperature, *i.e.*, $T_{\rm SG} = 0$.[19,20,21,22,23] Since applied magnetic fields make the SG transition even more unlikely, one has expected no phase transition to occur in applied fields, and hence, until quite recently, no extensive numerical simulation has ever been performed for the 3D Heisenberg SG in magnetic fields. Meanwhile, recent studies have revealed that the Heisenberg SG possesses an important physical ingredient absent in the Ising SG, *i.e.*, the *chirality*.[24,25,26,27,28,29,30,31,32] In the chirality scenario of Ref.[24,25], in particular, the chirality is claimed to be a hidden order parameter of the SG transition of real Heisenberg-like SG magnets: In the fully isotropic Heisenberg SG, the spin and the chirality, though they are coupled at short length scales, are eventually decoupled at long length scales, and the system exhibits a chiral-glass transition at a finite temperature without accompanying the standard SG order. The chiral-glass transition corresponds to the spontaneous breaking of the Z_2 spin-reflection symmetry with preserving the $SO(3)$ spin-proper-rotation symmetry. In the more realistic weakly anisotropic system, the Heisenberg spin, decoupled from the chirality in the isotropic system, is "recoupled" to the chirality at long length scales via the random magnetic anisotropy. The SG order of the weakly anisotropic Heisenberg SG is then dictated at long length scales by the chirality ordering of the isotropic system. Some numerical support of such a spin-chirality decoupling-recoupling scenario was already reported in zero field.[24,25,26,27,28]

By contrast, some other groups claimed that the chiral-glass transition of the 3D isotropic Heisenberg SG already accompanied the standard SG order, which means that the standard SG order occurs at a finite temperature simultaneously with the chirality.[33,34,35,36] Note that this is in contrast to the earlier belief in the community that the SG transition occurs only at $T = 0$ in the 3D Heisenberg SG. Ref.[29] maintains, however, that the SG order occurs at a temperature lower than the chiral-glass transition temperature, *i.e.*, $T_{\rm CG} > T_{\rm SG} \geq 0$, and the controversy remains.

Recently, the present authors performed the first extensive MC simulation of the 3D Heisenberg SG in magnetic fields, and have observed that the chiral-glass transition, essentially of the same character as in the zero-field one, occurs at a finite temperature even in magnetic fields.[30,31] The chiral-glass transition line in the temperature-magnetic field phase diagram turned out to have a striking resemblance to the GT-line observed experimentally, although the nature of the transition is entirely different from the mean-field GT-line. Note that the fully isotropic Heisenberg SG in fields possesses the global $Z_2 \times SO(2)$ symmetry, the chiral Z_2 referring to the global spin-reflection with respect to the plane containing the magnetic-field axis, and the $SO(2)$ referring to the global spin-rotation around the magnetic-field axis.

In the more realistic case of the weakly anisotropic Heisenberg SG, by contrast, there no longer remains any global symmetry in fields. Hence, from symmetry, the situation is the same as that of the well-studied Ising SG. Meanwhile, in view of the fact that the Heisenberg SG possesses the nontrivial chiral degree of freedom which is totally absent in the Ising SG, the question of whether the ordering properties of the weakly anisotropic Heisenberg SG in fields are essentially the same as those of the Ising SG in fields seems not so trivial. This question is further promoted by the apparently contradicting experimental observations on the Ising-like and weakly anisotropic Heisenberg-like SGs.[2,3,4]

In the present paper, we study both the spin-glass and the chiral-glass orderings of the weakly anisotropic Heisenberg SG in magnetic fields by extensive equilibrium Monte Carlo (MC) simulations[32]. We find a clear numerical evidence that a finite-temperature RSB transition occurs in the chiral sector, which also accompanies the simultaneous SG order. Thus, in spite of the similarity in the symmetry properties, the ordering properties of the weakly anisotropic Heisenberg SG model turn out to be quite different from those of the standard Ising SG. This highlights the importance of the chirality.

The paper is organized as follows. In §2, we introduce our model and explain the details of the MC simulation. Various physical quantities calculated in the simulation are defined in §3, and the results of our numerical simulation are presented in §4. In §5, we perform the scaling analysis of the critical properties of the transition, and construct a phase diagram of the model in the temperature - magnetic field plane. Section 6 is devoted to summary and discussion.

II. THE MODEL AND THE METHOD

In this section, we introduce our model and explain some of the details of our numerical method. The model we consider is the isotropic classical Heisenberg model on a 3D simple cubic lattice defined by the Hamiltonian,

$$\mathcal{H} = -\sum_{<ij>} (J_{ij} \boldsymbol{S}_i \cdot \boldsymbol{S}_j + \sum_{\mu,\nu=x,y,z} D_{ij}^{\mu\nu} S_{i\mu} S_{j\nu}) - H \sum_{i=1}^{N} S_{iz} \quad , \tag{1}$$

where $\boldsymbol{S}_i = (S_{ix}, S_{iy}, S_{iz})$ is a three-component unit vector, and H is the intensity of magnetic field applied along the z direction. The isotropic nearest-neighbor exchange coupling J_{ij} is assumed to take either the value J or $-J$ with equal probability, while the nearest-neighbor random exchange anisotropy $D_{ij}^{\mu\nu}$'s ($\mu,\ \nu$=x, y, z are spin-component indices) are assumed to be uniformly distributed in the range $[-D : D]$, where D is the typical intensity of the anisotropy. We impose the relation $D_{ij}^{\mu\nu} = D_{ji}^{\mu\nu} = D_{ij}^{\nu\mu}$.

We perform equilibrium MC simulations on this model. In the present simulation, we fix $D/J = 0.05$, which is a typical value of D of real Heisenberg-like SG materials. Simulations are then performed for a variety of field intensities in the range $H/J = 0.02 - 3.0$. The lattices studied are simple-cubic lattices with $N = L^3$ sites with $L = 4$, 6, 8, 10, 12 and 16 with periodic boundary conditions. Sample average is taken over 64-800 independent bond realizations, depending on the system size L and the field intensity H. Limited amount of data are also taken for $L = 20$ in some cases (32 samples) to check the size dependence of physical quantities.

To facilitate efficient thermalization, we combine the standard heat-bath method with the temperature-exchange technique.[37] The temperature-exchange trial is performed every heat-bath sweep. Typically, for the size $L = 16$ ($L = 20$), we discard initial 8×10^5 (13×10^5) heat-bath sweeps and the temperature-exchange trials for equilibration, and use subsequent 8×10^5 (13×10^5) heat-bath sweeps and the temperature-exchange trials in calculating various physical quantities. Care is taken to be sure that the system is fully equilibrated. Equilibration is checked by the following procedures: First, we monitor the system to travel back and forth many times during the

TABLE I: Details of our MC simulations. H/J represents the magnetic-field intensity, L the lattice size, $N_{\rm s}$ the total number of samples, $N_{\rm T}$ the total number of temperature points used in the temperature-exchange run, $T_{\rm max}/J$ and $T_{\rm min}/J$ the maximum and minimum temperatures in the temperature-exchange run.

H/J	L	$N_{\rm s}$	$N_{\rm T}$	$T_{\rm max}/J$	$T_{\rm min}/J$
0.05	4	800	26	0.475	0.085
	6	800	26	0.475	0.085
	8	600	26	0.475	0.113
	10	384	42	0.40	0.115
	12	256	52	0.40	0.115
	16	180	50	0.35	0.12
	20	32	50	0.35	0.1775
0.5	4	400	26	0.475	0.085
	6	400	26	0.475	0.085
	8	400	26	0.475	0.113
	10	300	42	0.40	0.115
	12	256	52	0.40	0.115
	16	64	50	0.35	0.12
	20	32	50	0.35	0.1775
3.0	4	400	26	0.475	0.085
	6	400	26	0.475	0.085
	8	400	26	0.475	0.113
	10	300	42	0.40	0.115
	12	256	52	0.40	0.115
	16	64	50	0.35	0.125

the temperature-exchange process (typically more than 10 times) between the maximum and minimum temperature points, and at the same time check that the relaxation due to the standard heat-bath updating is reasonably fast at the highest temperature, whose relaxation time is of order 10^2 Monte Carlo steps per spin (MCS). This guarantees that different parts of the phase space are sampled in each "cycle" of the temperature-exchange run. Second, we check the stability of the results against at least three times longer runs for a subset of samples. Error bars of physical quantities are estimated by the sample-to-sample statistical fluctuation over the bond realizations. Further details of our MC simulations are given in Table I.

III. PHYSICAL QUANTITIES

In this section, we define various physical quantities calculated in our simulations.

A. Chirality-related quantities

We begin with the definition of the chirality. The local chirality at the i-th site and in the μ-th direction, $\chi_{i\mu}$, is defined for three neighboring Heisenberg spins by the scalar

$$\chi_{i\mu} = \boldsymbol{S}_{i+\boldsymbol{e}_\mu} \cdot (\boldsymbol{S}_i \times \boldsymbol{S}_{i-\boldsymbol{e}_\mu}), \tag{2}$$

where $\boldsymbol{e}_\mu$ ($\mu = x, y, z$) denotes a unit vector along the μ-th axis. By this definition, there are in total $3N$ local chiral variables in the system. The local chirality amplitude is then defined by

$$\bar{\chi} = \sqrt{\frac{1}{3N} \sum_{i=1}^{N} \sum_{\mu=x,y,z} [\langle \chi_{i\mu}^2 \rangle]} \ , \tag{3}$$

where $\langle \cdots \rangle$ represents the thermal average and $[\cdots]$ represents the average over the bond disorder. The local chirality amplitude gives us the information of the extent of the non-coplanarity of local spin structures.

By considering two independent systems ("replicas") described by the same Hamiltonian, one can define an overlap of the chiral variable via the relation,

$$q_\chi = \frac{1}{3N}\sum_{i=1}^{N}\sum_{\mu=x,y,z}\chi_{i\mu}^{(a)}\chi_{i\mu}^{(b)} \quad , \tag{4}$$

where $\chi_{i\mu}^{(a)}$ and $\chi_{i\mu}^{(b)}$ represent the chiral variables of the replicas "a" and "b", respectively. In our simulations, we prepare the two replicas a and b by running two independent sequences of systems in parallel with different spin initial conditions and different sequences of random numbers.

Since the present model does not possess any global symmetry, an odd quantity $[\langle q_\chi\rangle]$ is generally non-zero even in the hight-temperature phase. Taking this effect into consideration, the chiral-glass order parameter may be defined by

$$\tilde{q}_\chi^{(2)} = [\langle(q_\chi - [\langle q_\chi\rangle])^2\rangle] \quad . \tag{5}$$

The associated chiral-glass susceptibility, normalized by the local amplitude $\bar{\chi}$, is defined by

$$\tilde{\chi}_\chi = 3N\frac{\tilde{q}_\chi^{(2)}}{\bar{\chi}^4} \quad . \tag{6}$$

The Binder ratio of the chirality is defined by

$$g'_\chi = \frac{1}{2}\left(3 - \frac{\tilde{q}_\chi^{(4)}}{(\tilde{q}_\chi^{(2)})^2}\right) \quad , \tag{7}$$

where

$$\tilde{q}_\chi^{(4)} = [\langle(q_\chi - [\langle q_\chi\rangle])^4\rangle] \quad . \tag{8}$$

Here, g'_χ is normalized so that, in the thermodynamic limit, it vanishes in the high-temperature phase and gives unity in the ordered phase if the ordered state is non-degenerate. The distribution function of the chiral overlap q_χ is defined by

$$P_\chi(q'_\chi) = [\langle\delta(q'_\chi - q_\chi)\rangle] \quad . \tag{9}$$

We consider the Fourier-transformed two-point chiral-glass correlation function $\mathcal{C}_{\rm CG}^{\mu\nu}(\boldsymbol{k})$ between the two local chiral variables in the μ-th and in the ν-th directions. While one can define various types of correlation functions depending on the relative directions of the chiral variables (μ,ν) and the direction of $\boldsymbol{k}$, we consider here the parallel component $\mathcal{C}_{\rm CG}^{\parallel}(\boldsymbol{k})$ where μ and ν are both parallel with $\boldsymbol{k}$. Here, we put $\boldsymbol{k}$ parallel with the x-direction, $\boldsymbol{k} = (k,0,0)$, so that $\mu = \nu = x$. Then, $\mathcal{C}_{\rm CG}^{\parallel}(\boldsymbol{k})$ can be written in terms of the k-dependent chiral overlap $q_\chi(\boldsymbol{k})$,

$$\mathcal{C}_{\rm CG}^{\parallel}(\boldsymbol{k}) = [< |q_\chi(\boldsymbol{k})|^2 >], \tag{10}$$

$$q_\chi(\boldsymbol{k}) = \frac{1}{N}\sum_{i=1}^{N}\chi_{ix}^{(a)}\chi_{ix}^{(b)}\exp(i\boldsymbol{k}\cdot\boldsymbol{r}_i), \tag{11}$$

where $\boldsymbol{r}_i = (x_i, y_i, z_i)$ denotes the position vector of the chiral variable at the i-th site. The associated chiral correlation length, ξ_χ, is defined by,

$$\xi_\chi = \frac{1}{2\sin(k_{\rm m}/2)}\sqrt{\frac{\mathcal{C}_{\rm CG}^{\parallel}(\boldsymbol{0})}{\mathcal{C}_{\rm CG}^{\parallel}(\boldsymbol{k}_{\rm m})} - 1} \quad , \tag{12}$$

where $\boldsymbol{k}_{\rm m} = (2\pi/L, 0, 0)$ is a wavevector of the minimum magnitude.

In order to study the equilibrium dynamics of the model, we compute the equilibrium autocorrelation function of the chirality defined by

$$\tilde{C}'_\chi(t) \;=\; \left[\left\langle\frac{1}{3N}\sum_{i=1}^{N}\sum_{\mu=x,y,z}\chi_{i\mu}(t_0)\chi_{i\mu}(t+t_0)\right\rangle\right] \;-\; [\langle q_\chi\rangle] \quad , \tag{13}$$

where the "time" t is measured in units of MCS. This chiral autocorrelation function is an "odd" quantity not invariant under the global flipping of the chirality. The corresponding "even" time correlation functions which is invariant under the global flipping of the chirality, may be defined by

$$\tilde{q}_\chi^{(2)'}(t) \;=\; \left[\left\langle\left(\frac{1}{3N}\sum_{i=1}^{N}\sum_{\mu=x,y,z}\chi_{i\mu}(t_0)\chi_{i\mu}(t+t_0)\right)^2\right\rangle\right] \;-\; [\langle q_\chi^2\rangle] \quad . \tag{14}$$

In displaying the data, we normalize these time correlation functions by their values at a unit time $t = 1$, *i.e.*, we put

$$C_\chi(t) = C'_\chi(t)/C'_\chi(1), \qquad \tilde{q}_\chi^{(2)}(t) = \tilde{q}_\chi^{(2)'}(t)/\tilde{q}_\chi^{(2)'}(1). \tag{15}$$

Note that in the above definitions of the time-correlation functions (13) and (14), the second terms, $[\langle q_\chi\rangle]$ and $[\langle q_\chi^2\rangle]$, have been subtracted, which are nonzero even in the high-temperature phase in the $L \to \infty$ limit due to the absence of any global symmetry. This subtraction guarantees that both $\tilde{C}_\chi(t)$ and $\tilde{q}_\chi^{(2)}(t)$ decay to zero as $t \to \infty$ in the high-temperature phase. In the possible ordered phase, by contrast, both $\tilde{C}_\chi(t)$ and $\tilde{q}_\chi^{(2)}(t)$ decay to zero *if* the ordered state does not accompany the RSB, but tend to finite positive values *if* the ordered state accompanies the RSB. The latter property arises because, in the presence of RSB, the $t \to \infty$ limits of the first terms of Eqs.(13) and (14) are generally greater than the second terms, $[\langle q_\chi\rangle]$ and $[\langle q_\chi^2\rangle]$.

In computing the first terms of Eqs.(13) and (14), the simulation is performed according to the standard heat-bath updating without the temperature-exchange procedure, while the starting spin configuration at $t = t_0$ is taken from the equilibrium spin configurations generated in our temperature-exchange MC runs. The second terms of Eqs.(13) and (14) are evaluated from the temperature-exchange MC runs.

B. Spin-related quantities

As in the case of the chirality, it is convenient to define an overlap variable for the Heisenberg spin. In this case, the overlap might naturally be defined as a *tensor* variable $q_{\mu\nu}$ between the μ and ν components (μ, ν=x, y, z) of the Heisenberg spin,

$$q_{\mu\nu} = \frac{1}{N}\sum_{i=1}^{N} S_{i\mu}^{(a)} S_{i\nu}^{(b)} \quad , \quad (\mu = x, y, z), \tag{16}$$

where $\boldsymbol{S}_i^{(a)}$ and $\boldsymbol{S}_i^{(b)}$ are the i-th Heisenberg spins of the replicas a and b, respectively.

In terms of these tensor overlaps, the "longitudinal" (parallel to the applied field) and the "transverse" (perpendicular to the applied field) SG order parameters may be defined by

$$\tilde{q}_{\rm L}^{(2)} = [\langle(q_{\rm L} - [\langle q_{\rm L}\rangle])^2\rangle], \qquad q_{\rm L} = q_{zz} \quad , \tag{17}$$

$$\tilde{q}_{\rm T}^{(2)} = [\langle(q_{\rm T} - [\langle q_{\rm T}\rangle])^2\rangle], \qquad q_{\rm T} = \sum_{\mu=x,y} q_{\mu\mu} = q_{xx} + q_{yy} \quad . \tag{18}$$

Note that as in the case of the chirality, the expectation value of the first moment has been subtracted. We also consider the spin-glass susceptibility for the transverse spin component defined by,

$$\tilde{\chi}_{\rm T} = N\tilde{q}_{\rm T}^{(2)} \quad . \tag{19}$$

The longitudinal and the transverse Binder ratios are defined, respectively, by

$$g'_{\rm L} \;=\; \frac{1}{2}\left(3 - \frac{\tilde{q}_{\rm L}^{(4)}}{(\tilde{q}_{\rm L}^{(2)})^2}\right) \quad , \tag{20}$$

$$g'_{\rm T} \;=\; \frac{1}{2}\left(3 - \frac{\tilde{q}_{\rm T}^{(4)}}{(\tilde{q}_{\rm T}^{(2)})^2}\right) \quad , \tag{21}$$

where

$$\tilde{q}_{\rm L}^{(4)} \;=\; [\langle(q_{\rm L} - [\langle q_{\rm L}\rangle])^4\rangle] \quad , \tag{22}$$

$$\tilde{q}_{\rm T}^{(4)} \;=\; [\langle(q_{\rm T} - [\langle q_{\rm T}\rangle])^4\rangle] \quad . \tag{23}$$

Here, $g'_{\rm L}$ and $g'_{\rm T}$ are normalized so that, in the thermodynamic limit, they vanish in the high-temperature phase and give unity in the ordered state if the ordered state is non-degenerate.

The full spin-overlap distribution function may be defined in the tensor space with $3 \times 3 = 9$ components. Here, we consider the spin-overlap distribution function for the longitudinal and the transverse components, each defined by

$$P_{\rm s}(q'_{\rm L}) = [\langle \delta(q'_{\rm L} - q_{\rm L})\rangle] \quad , \tag{24}$$

$$P_{\rm s}(q'_{\rm T}) = [\langle \delta(q'_{\rm T} - q_{\rm T})\rangle] \quad , \tag{25}$$

where $q_{\rm L}$ and $q_{\rm T}$ are defined by Eqs.(17) and (18), respectively. In the possible SG ordered state of the *isotropic* system, $P_{\rm s}(q_{\rm T})$ develops a non-trivial shape in the thermodynamic limit due to the fact that the transverse-spin-overlap $q_{\rm T}$ transforms non-trivially under the global spin rotation: See Refs.[38] and[39] for details. But here, the system is anisotropic so that no non-trivial structure arising from the uniform global spin-rotation is expected to arise in $P_{\rm s}(q_{\rm T})$ in the thermodynamic limit.

We consider the Fourier-transformed spin-glass correlation functions both for the longitudinal and the transverse components, $\mathcal{C}_{\rm L}(\boldsymbol{k})$ and $\mathcal{C}_{\rm T}(\boldsymbol{k})$, which can be written in terms of the k-dependent longitudinal and transverse spin-overlaps, $q_{\rm L}(\boldsymbol{k})$ and $q_{\rm T}(\boldsymbol{k})$, as,

$$\mathcal{C}_{\rm L}(\boldsymbol{k}) = [< |q_{\rm L}(\boldsymbol{k})|^2 >], \qquad \mathcal{C}_{\rm T}(\boldsymbol{k}) = [< |q_{\rm T}(\boldsymbol{k})|^2 >], \tag{26}$$

with

$$q_{\rm L}(\boldsymbol{k}) = \frac{1}{N}\sum_{i=1}^{N} S_{iz}^{(a)} S_{iz}^{(b)} \exp(i\boldsymbol{k}\cdot\boldsymbol{r}_i), \qquad q_{\rm T}(\boldsymbol{k}) = \frac{1}{N}\sum_{i=1}^{N} \boldsymbol{S}_{i{\rm T}}^{(a)} \cdot \boldsymbol{S}_{i{\rm T}}^{(b)} \exp(i\boldsymbol{k}\cdot\boldsymbol{r}_i). \tag{27}$$

where $\boldsymbol{S}_{i{\rm T}} = (S_{ix}, S_{iy})$ represents the transverse (xy) component of the Heisenberg spin. The associated longitudinal and the transverse spin correlation lengths, $\xi_{\rm L}$ and $\xi_{\rm T}$, are defined by

$$\xi_{\rm L} = \frac{1}{2\sin(k_{\rm m}/2)}\sqrt{\frac{\mathcal{C}_{\rm L}(\boldsymbol{0})}{\mathcal{C}_{\rm L}(\boldsymbol{k}_{\rm m})} - 1} \quad , \tag{28}$$

$$\xi_{\rm T} = \frac{1}{2\sin(k_{\rm m}/2)}\sqrt{\frac{\mathcal{C}_{\rm T}(\boldsymbol{0})}{\mathcal{C}_{\rm T}(\boldsymbol{k}_{\rm m})} - 1} \quad , \tag{29}$$

respectively.

The spin autocorrelation functions are defined both for the longitudinal and the transverse components by

$$\tilde{C}_{\rm L}(t) = \tilde{C}'_{\rm L}(t)/\tilde{C}'_{\rm L}(1), \quad \tilde{C}'_{\rm L}(t) \;=\; \frac{1}{N}\sum_{i=1}^{N}[\langle S_{iz}(t_0)S_{iz}(t+t_0)\rangle] - [\langle q_{\rm L}\rangle] \quad , \tag{30}$$

$$\tilde{C}_{\rm T}(t) = \tilde{C}'_{\rm T}(t)/\tilde{C}'_{\rm T}(1), \quad \tilde{C}'_{\rm T}(t) \;=\; \frac{1}{N}\sum_{i=1}^{N}[\langle \boldsymbol{S}_{i{\rm T}}(t_0)\cdot\boldsymbol{S}_{i{\rm T}}(t+t_0)\rangle] - [\langle q_{\rm T}\rangle] \quad . \tag{31}$$

The second terms, $[\langle q_{\rm L}\rangle]$ and $[\langle q_{\rm T}\rangle]$, have been subtracted in the same context as in the definition of $\tilde{C}_\chi(t)$ for the chirality. These spin autocorrelation functions are computed in the same way as the chiral autocorrelation functions, and are normalized at their values at a unit time $t = 1$. The corresponding "even" time correlation functions can also be defined, though we skip their definitions here.

IV. NUMERICAL RESULTS

In this section, we show the results of our MC simulations on the anisotropic Heisenberg SG with $D/J = 0.05$.

A. Time correlation functions of the chirality

In Fig.1, we show the MC time dependence of the chiral autocorrelation function $\tilde{C}_\chi(t)$ for the size $L = 16$ on log-log plots, for the fields (a) $H/J = 0.05$, (b) $H/J = 0.5$ and (c) $H/J = 3.0$, respectively. In the case $H/J = 0.05$, we have checked that, in the time range shown, the data can be regarded as those of the bulk, since no appreciable size effect is discernible between the data of $L = 16$ and $L = 20$, the latter data being shown with lines in the figure. In Fig.2, we show the MC time dependence of the corresponding even quantities, $\tilde{q}_\chi^{(2)}(t)$, for the fields (a) $H/J = 0.05$, (b) $H/J = 0.5$ and (c) $H/J = 3.0$, respectively. As can clearly be seen from these figures, in the investigated time range, the observed behavior of $\tilde{C}_\chi(t)$ is essentially the same as that of $\tilde{q}_\chi^{(2)}(t)$.

For the field $H/J = 0.05$, as can be seen from the Figs. 1(a) and 2(a), $\tilde{C}_\chi(t)$ and $\tilde{q}_\chi^{(2)}(t)$ exhibit either a down-bending or an up-bending behavior depending on whether the temperature is higher or lower than a borderline value $T/J \simeq 0.21$. while just at this borderline temperature a straight-line behavior corresponding to a power-law decay is observed. This indicates that the chirality exhibits a phase transition into the low-temperature ordered phase where the replica symmetry is spontaneously broken. In the case of $H/J = 0.5$, as can be seen from Figs.1(b) and 2(b), the data at $T/J \lesssim 0.24$ show a slight up-bending tendency at a short time $t \simeq 10^2$ while the data at $T/J \gtrsim 0.21$ show a gradual down-bending tendency at longer times $t \simeq 10^3$, and the chiral transition temperature appears to lie somewhere between $T/J \simeq 0.21$ and 0.24. The transverse spin autocorrelation, which is to be shown in Fig.3(c) below, however, suggests the transition temperature $T_g \simeq 0.20 - 0.21$. Then, we finally estimate the transition temperature $T_g/J = 0.21 \pm 0.02$ for $H/J = 0.5$ (see below). In the case $H/J = 3.0$, by contrast, $\tilde{C}_\chi(t)$ and $\tilde{q}_\chi^{(2)}(t)$ always exhibits a down-bending behavior in the temperature range studied, suggesting the absence of a phase transition, at least in the temperature range $T/J \geq 0.125$.

Since very much similar behaviors are observed in $\tilde{C}_\chi(t)$ and in $\tilde{q}_\chi^{(2)}(t)$, we shall show in the following subsections the data of the autocorrelation function $\tilde{C}(t)$ only.

B. Time correlation functions of the spin

In Figs.3, we show for the fields $H/J = 0.05$ and 0.5 the MC time dependence of the autocorrelation functions of the transverse component of the spin $\tilde{C}_{\rm T}(t)$, Figs.(a) and (c), and those of the longitudinal component of the spin $\tilde{C}_{\rm L}$, Figs.(b) and (d). Finite-size effect evaluated from the difference between the $L = 16$ and $L = 20$ data turns out to be rather small (but not completely negligible) in the longitudinal component, whereas it is more appreciable in the transverse component. Although a finite-size effect is not completely negligible here, the autocorrelation functions of the spin for $H/J = 0.05$ turn out to behave quite similarly to those of the chirality. Namely, both $\tilde{C}_{\rm L}(t)$ and $\tilde{C}_{\rm T}(t)$ exhibit either a down-bending or an up-bending behavior depending on whether the temperature is higher or lower than the borderline value $T/J \simeq 0.21$, while just at this borderline temperature a straight-line behavior corresponding a power-law decay is observed. This indicates that the spin exhibits an RSB transition at the same temperature where the chirality exhibits an RSB transition. The simultaneous occurrence of the spin and the chirality orderings is quite natural in the presence of the random anisotropy.

For the field $H/J = 0.5$, the transverse component $\tilde{C}_{\rm T}(t)$ shown in Fig.3(c) exhibits a rather clear up-bending/down-bending behavior with the borderline temperature $T/J \simeq 0.20 - 0.21$, which might be compared with the less clear behavior of $\tilde{C}_\chi(t)$ where the transition temperature appears to lie somewhere between $T/J \simeq 0.21 - 0.24$. Since the transition here is expected to be a simultaneous spin and chiral transition, we now estimate the transition temperature of the field $H/J = 0.5$ to be $T_g = 0.21 \pm 0.02$. Meanwhile, the longitudinal autocorrelation function $\tilde{C}_{\rm L}(t)$ for $H/J = 0.5$ exhibits a much noisier behavior as shown in Fig.3(d). This is because, in large fields, the second term of Eq.(30), $[\langle q_{\rm L} \rangle]$, becomes large, while the longitudinal spin correlation function itself becomes small in magnitude which is obtained as a difference between the two large numbers. Note that the up-bending behavior is discernible at a short time $t \simeq 10^2$, which is also observed in the chiral autocorrelation in a less pronounced manner. In any case, due to the noisiness, it seems not possible to identify the transition point from Fig.3(d).

From the behaviors of the chiral and the spin autocorrelation functions shown above, we conclude that the spin and the chirality exhibit an RSB transition simultaneously at a finite temperature $T_g/J = 0.21 \pm 0.02$ for both the fields $H/J = 0.05$ and 0.5. The estimated transition temperature $T_g/J = 0.21(2)$ is lower than the transition temperature of the corresponding zero-field model with the same magnitude of anisotropy, *i.e.*, $T_g/J \simeq 0.24$,[28,29] indicating that applied magnetic fields suppress the spin-glass (chiral-glass) ordering for weaker fields. Indeed, this is exactly the feature expected for the experimental AT-line. Interestingly, the estimated transition temperature under fields, $T_g/J \simeq 0.21$, comes very close to the chiral-glass transition temperature of the fully isotropic model in zero field, which was estimated to be $T_{\rm CG}/J \simeq 0.20$.[29] This is exactly the feature expected for the experimental

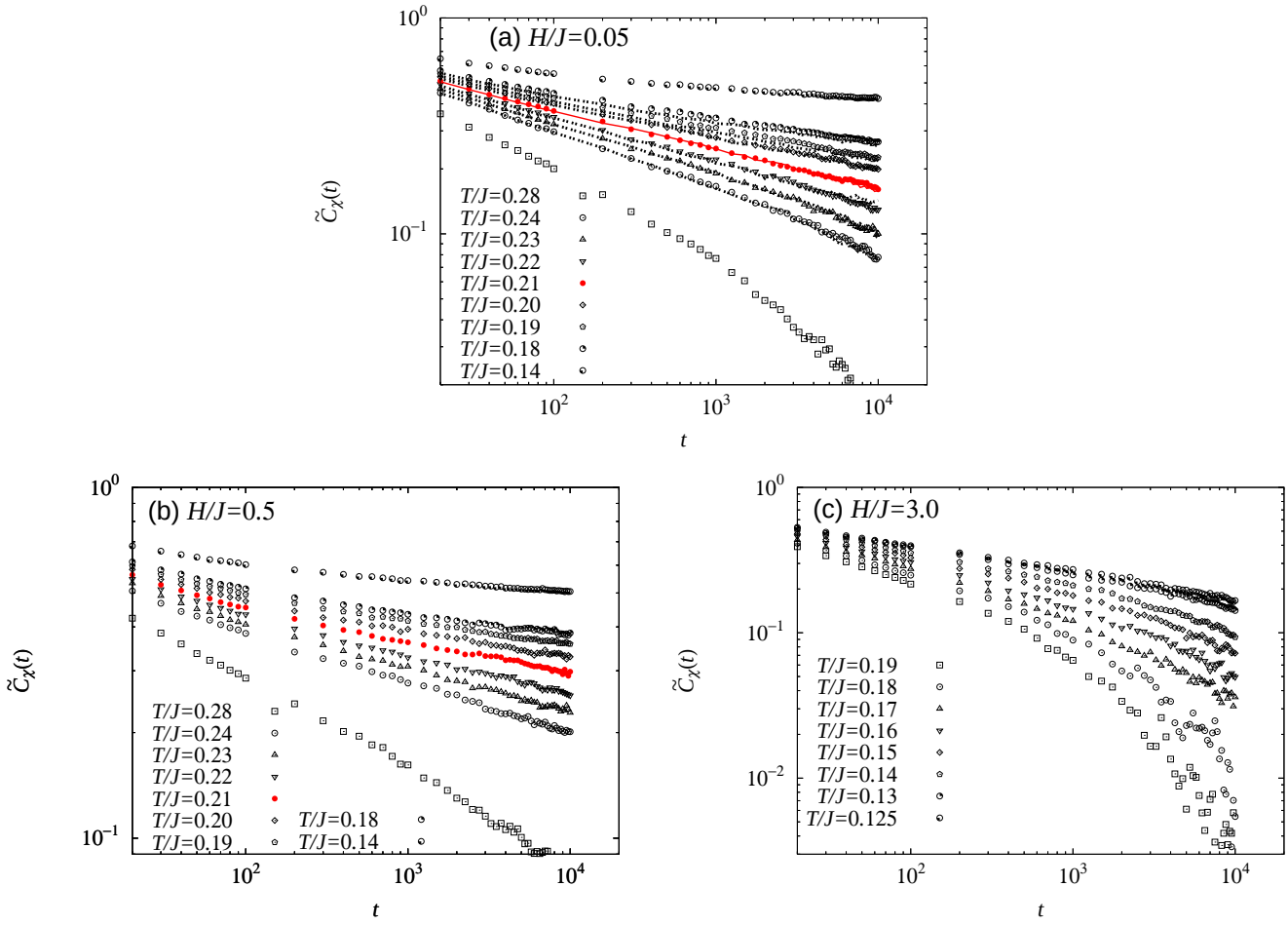

FIG. 1: (Color online) Temporal decay of the autocorrelation function of the chirality $\tilde{C}_\chi(t)$ defined by Eqs. (13) and (15), for the fields (a) $H/J = 0.05$, (b) $H/J = 0.5$ and (c) $H/J = 3.0$. The lattice size is $L = 16$. The data at $T = T_g$ are given in red (by filled symbols). In Fig.(a), in order to check the finite-size effect, the data of $L = 20$ are plotted with lines at temperatures $T/J = 0.18$-0.24 with an interval of 0.01. The estimated transition temperature is $T_g/J \simeq 0.21$ both for $H/J = 0.05$ and $H/J = 0.5$.

GT-line. Hence, the suppression of $T_g(H)$ due to weaker fields (AT-line) as well as the robustness of it with respect to stronger fields (GT-line) are consistent with the experimental observation for the weakly anisotropic Heisenberg-like SGs.[1,3,4]

C. Comparison with the autocorrelation functions of the 3D Ising SG in fields

For comparison, we also calculate the autocorrelation function of the spin $\tilde{C}_{\rm L}(t)$ defined by Eq. (30) for the 3D Ising SG with the $\pm J$ coupling for the field $H/J = 0.05$. Note that the Ising SG in fields shares the same symmetry property as the anisotropic Heisenberg SG in fields, *i.e.*, the absence of any global symmetry. Nevertheless, *the Ising SG does not possess any chiral degree of freedom*. Thus, the question of whether the 3D Ising SG behaves either similarly or differently from the weakly anisotropic Heisenberg SG would be of special interest.

The data of $\tilde{C}_{\rm L}(t)$ of the Ising SG are shown in Fig.4 for the size $L = 20$. As can be seen from figure, the behavior of $\tilde{C}_{\rm L}(t)$ of the Ising SG differs significantly from that of the weakly anisotropic Heisenberg SG. Although the temperature range studied is as low as about 60% of the zero-field transition temperature $T_g(H = 0)/J \simeq 1.1$, which is expected to be deep in the ordered state according to a tentative estimate of Ref.[18], no clear up-bending behavior as observed in the weakly anisotropic Heisenberg SG is observed here. Instead, $\tilde{q}^{(2)}_{\rm L}(t)$ and $\tilde{C}_{\rm L}(t)$ persistently exhibit an almost linear behavior even at the lowest temperature studied $T/J = 0.6$. This is illustrated in Fig.4(b) where the $\tilde{C}_{\rm L}(t)$ data at the two lowest temperatures studied are shown. A comparison of the $L = 20$ data with the $L = 16$

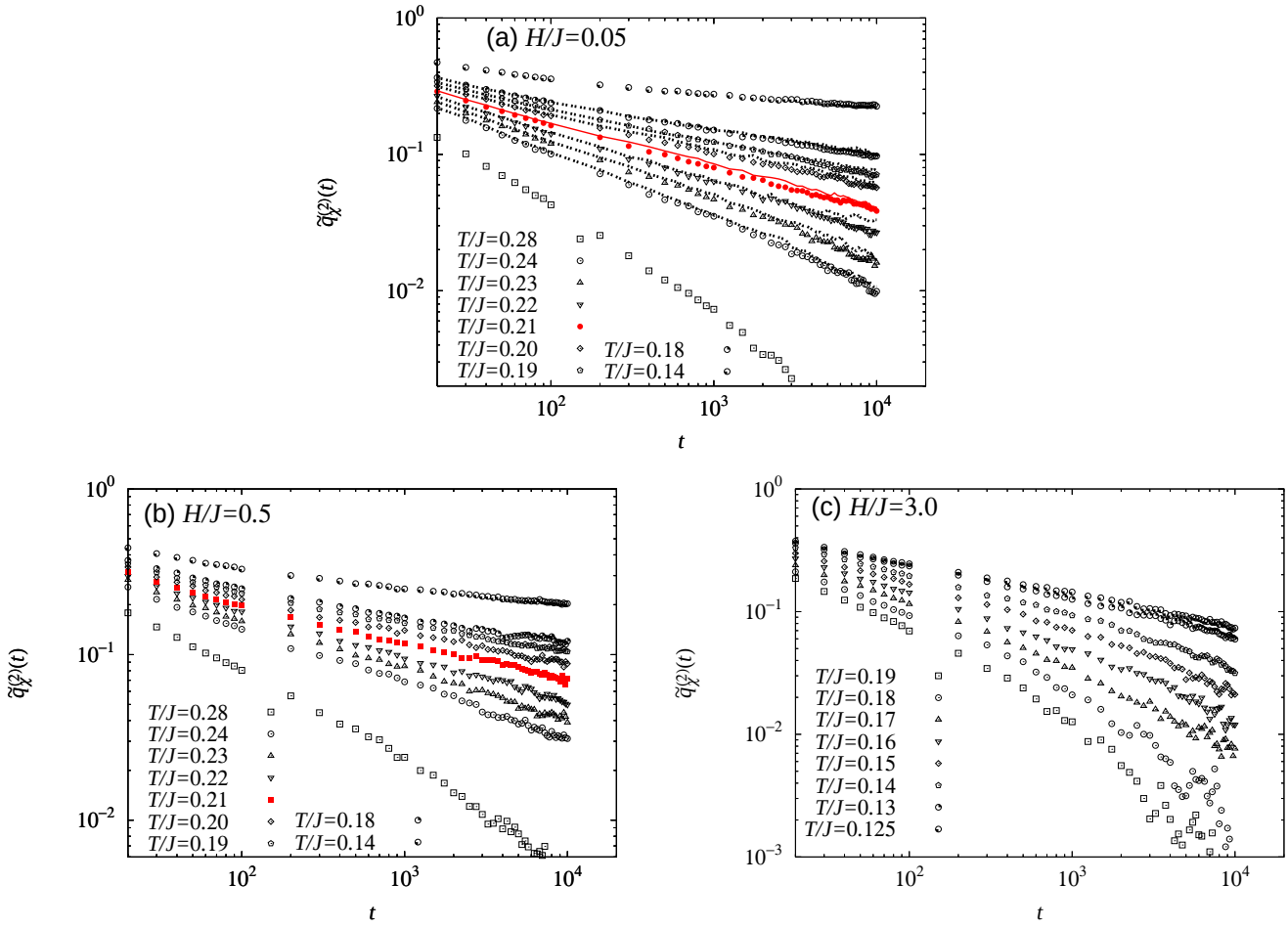

FIG. 2: (Color online) Temporal decay of the time-correlation function of the chirality $\tilde{q}^{(2)}_\chi(t)$ defined by Eqs.(14) and (15), for the fields (a) $H/J = 0.05$, (b) $H/J = 0.5$ and (c) $H/J = 3.0$. The lattice size is $L = 16$. The data at $T = T_g$ are given in red (by filled symbols). In Fig.(a), in order to check the finite-size effect, the data of $L = 20$ are plotted with lines at temperatures $T/J = 0.18$-0.24 with an interval of 0.01. The estimated transition temperature is $T_g/J \simeq 0.21$ both for $H/J = 0.05$ and $H/J = 0.5$.

data indicates that some amount of finite-size effect still remains. Nevertheless, an almost linear behavior without any discernible up-bending tendency is robustly observed in common both for $L = 16$ and $L = 20$, suggesting that this feature is a bulk property.

D. The Binder ratio of the chirality

In Fig.5, we show the temperature- and size- dependence of the chiral Binder ratio g'_χ for the field $H/J = 0.05$. The data of g'_χ has a negative dip at a size-dependent temperature $T = T_{\rm dip}(L)$, which, with increasing L, tends to deepen and shift to lower temperatures. The existence of a persistent negative dip with increasing depth, is a sign of a phase transition occurring at $T = T_{\rm dip}(L = \infty)$. By extrapolating $T_{\rm dip}(L)$ to $L = \infty$, as shown in the inset of Fig.5, the bulk chiral-glass transition temperature is estimated to be $T_g/J = 0.22(2)$. The estimated transition temperature agrees well with the corresponding estimate based on the autocorrelation functions given above.

As argued in Ref.[27,31,40] for the isotropic case, the existence of a persistent negative dip is a sign of a one-step-like RSB transition. In the present anisotropic model under fields, there no longer exists a global spin-reflection symmetry in contrast to the isotropic model under fields. Hence, the behavior expected for g'_χ here might be the one for the one-step RSB system *without a reflection symmetry*. Such a system was theoretically analyzed in Ref.[41], where the behavior of the Binder ratio g'_χ in the thermodynamic limit was reported as shown in Fig.6.[41] Indeed, the overall behavior of our present g'_χ shown in Fig.6 seems consistent with such a behavior.

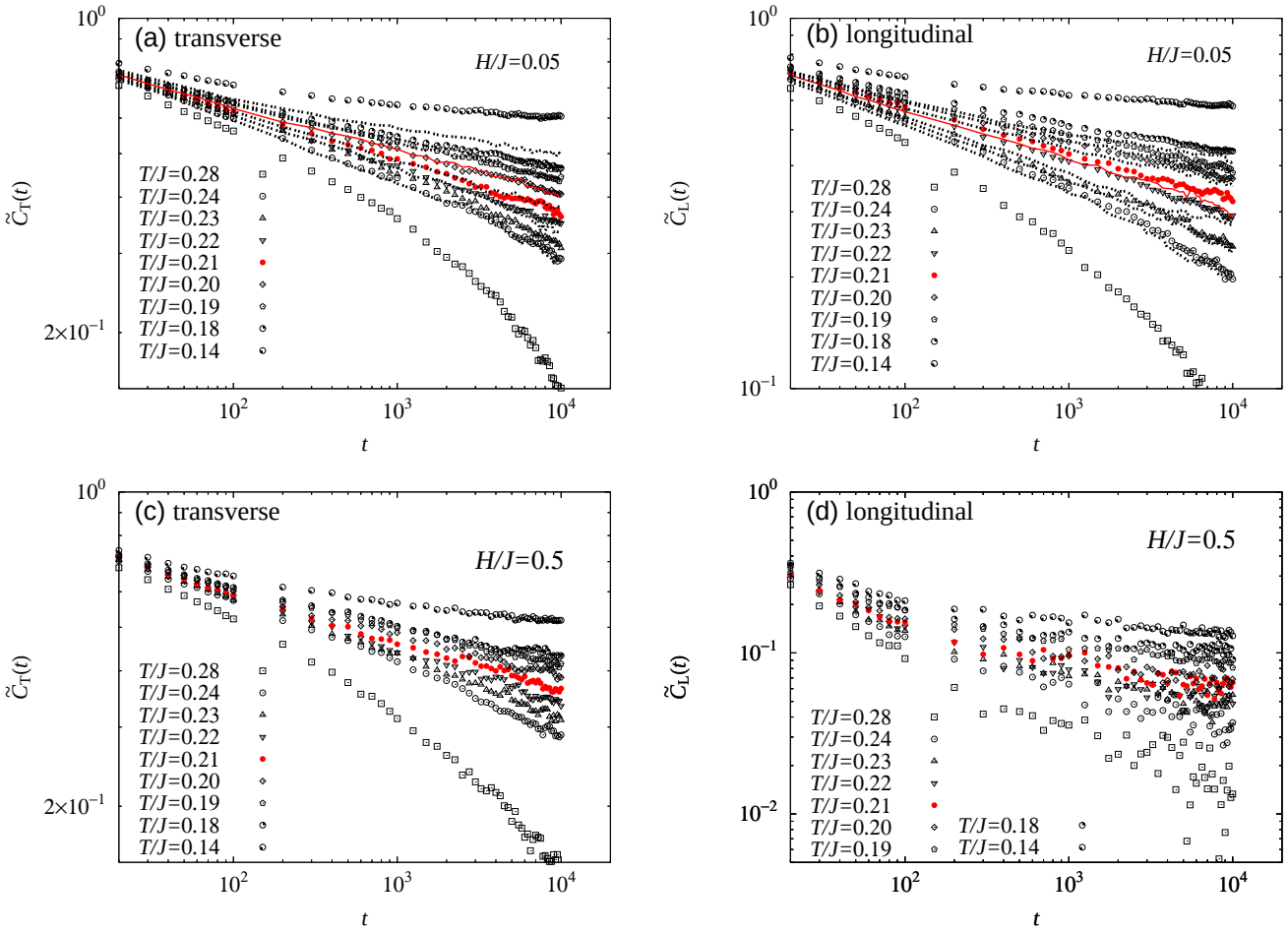

FIG. 3: (Color online) Temporal decay of the spin autocorrelation functions: (a) the transverse one $\tilde{C}_{\rm T}(t)$ for $H/J = 0.05$, (b) the longitudinal one $\tilde{C}_{\rm L}(t)$ for $H/J = 0.05$, (c) the transverse one for $H/J = 0.5$, and (d) the longitudinal one for $H/J = 0.5$. The lattice size is $L = 16$. The data at $T = T_g$ are given in red (by filled symbols). In the figures, in order to check the finite size effect, the data of $L = 20$ are plotted with lines at temperatures $T/J = 0.18$-0.24 with an interval of 0.01. The estimated transition temperatures is $T_g/J \simeq 0.21$ both for $H/J = 0.05$ and $H/J = 0.5$.

E. The Binder ratio of the spin

In Fig.7(a), we show the temperature and size dependence of the Binder ratio of the longitudinal component of the spin $g'_{\rm L}$ for the field $H/J = 0.05$. Although $g'_{\rm L}$ for smaller sizes $L \leq 12$ does not show any characteristic feature suggestive of a phase transition, the one for larger sizes $L \geq 16$ tends to exhibit a negative dip similar to the one as observed in the chiral Binder ratio g'_χ. Then, for large enough L, the overall shape of $g'_{\rm L}$ would be similar to that of g'_χ, although the one for smaller L is very different.

In Fig.7(b), we show the temperature and size dependence of the Binder ratio of the transverse component of the spin $g'_{\rm T}$ for the field $H/J = 0.05$. Although g'_T for smaller sizes $L \leq 12$ exhibits a single maximum with a crossing point occurring around $T/J \simeq 0.28$, the one for larger sizes $L \geq 16$ exhibits double maxima. The apparent crossing point observed for smaller sizes at $T/J \simeq 0.28$ disappears for larger lattices, indicating that it does not correspond to a true phase transition point. Among the two maxima of $g'_{\rm T}$ observed for $L \geq 16$, the one at a higher temperature is gradually suppressed with increasing L, while the one at a lower temperature tends to be enhanced. Presumably, in the $L \to \infty$ limit, the peak at a higher temperature will disappear, while the peak at a lower temperature will survive. Then, for large enough L, the overall shape of $g'_{\rm T}$ would be similar to that of g'_χ and $g'_{\rm L}$, although the one for smaller L is very different. Our observation here that the Binder ratio of the chirality, g'_χ, and those of the spin, $g'_{\rm L}$ and $g'_{\rm T}$, asymptotically show mutually similar behavior, which resembles the one depicted in Fig.6, seems consistent with the spin-chirality decoupling-recoupling scenario. Indeed, the recoupling

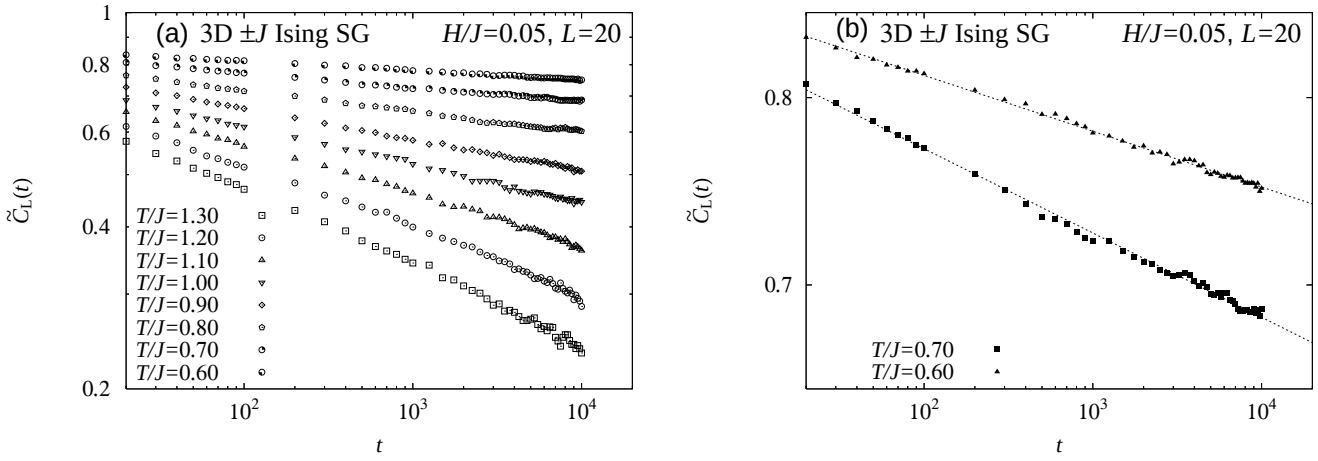

FIG. 4: Temporal decay of the spin autocorrelation function, defined by Eq. (30), of the $\pm J$ 3D Ising SG in a magnetic field of $H/J = 0.05$. The system size is $L = 20$ averaged over 100 samples. In (a), the data are plotted in the temperature range $T/J = 0.60 - 1.3$ with an interval of 0.1. The data of the two lowest temperatures $T/J = 0.60$ and 0.70 are shown in (b), together with the fitted straight lines. Even at the lowest temperature studied, no up-bending behavior is observed.

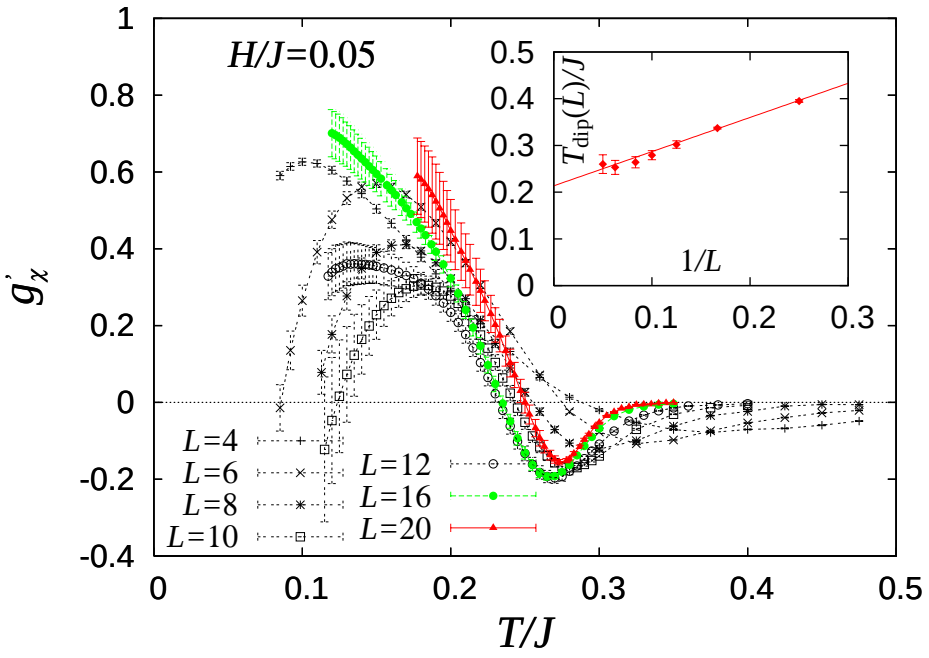

FIG. 5: (Color online) The temperature and size dependence of the Binder ratio of the chirality g'_χ for a field $H/J = 0.05$. In the inset, we show the reciprocal size dependence of the dip temperature of g'_χ. Dashed line represents a linear fit of the data. The bulk chiral-glass transition temperature is estimated to be $T_g/J = 0.22(2)$.

length-scale estimated in Ref.[29,38], $L_\times \simeq 20$, is consistent with the observed behavior.

F. Overlap distribution function of the chirality

We show in Figs.8 the size dependence of the overlap distribution function of the chirality, $P_\chi(q_\chi)$, for several cases, *i.e.*, (a) $H/J = 0.05$ and $T/J = 0.18$, (b) $H/J = 0.5$ and $T/J = 0.19$, (c) $H/J = 0.5$ and $T/J = 0.12$, and

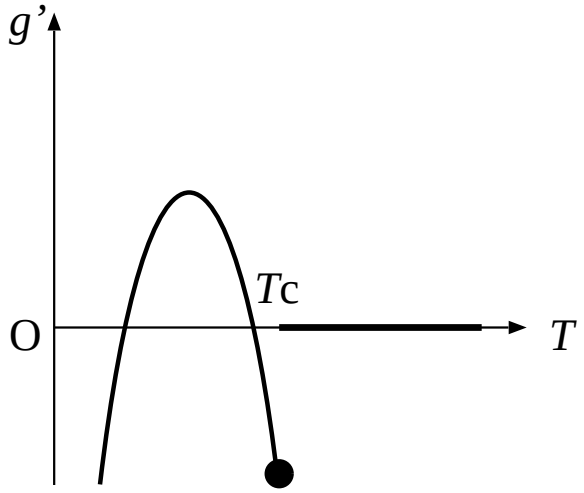

FIG. 6: A sketch of the typical temperature dependence of the Binder ratio g' in the thermodynamic limit, which is expected in a system without a reflection symmetry exhibiting a one-step RSB transition.

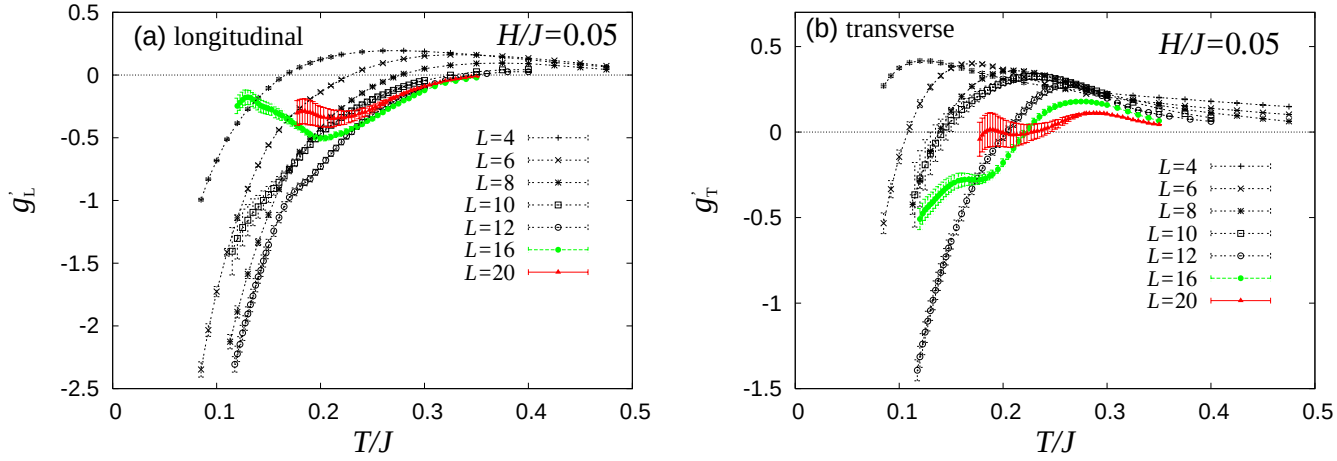

FIG. 7: (Color online) The temperature and size dependence of the Binder ratio of (a) the longitudinal component of the spin $g'_{\rm L}$, and of (b) the transverse component of the spin $g'_{\rm T}$, for a field $H/J = 0.05$.

(d) $H/J = 3.0$ and $T/J = 0.13$.

In the case $H/J = 0.05$, in addition to a primary peak corresponding to $q_\chi = q_\chi^{\rm EA} > 0$, which grows and sharpens with increasing L, there appears a second peak at around $q_\chi = 0$, which also grows and sharpens with increasing L. The existence of two distinct peaks, both growing and sharpening with increasing L, is a clear indication of the occurrence of RSB. As reported in Ref.[27], $P_\chi(q_\chi)$ in zero field exhibits a feature of a one-step-like RSB, *i.e.*, a central peak at $q_\chi = 0$ coexisting with self-overlap peaks at $q_\chi = \pm q_\chi^{\rm EA}$. The $P_\chi(q_\chi)$ observed here may be regarded as the in-field counterpart of the zero-field $P_\chi(q_\chi)$ with a feature of such a one-step-like RSB. Indeed, if one closely looks at $P_\chi(q_\chi)$ shown in Fig.8(a), one sees that a broad peak, which is a remnant of the $q_\chi = -q_\chi^{\rm EA}$ peak of the zero-field model, is discernible for smaller sizes $L \leq 8$, whereas, for larger sizes, this $q_\chi = -q_\chi^{\rm EA}$ peak disappears and the $q_\chi \simeq 0$ peak begins to grow. Interestingly, for the size $L = 8$, $P_\chi(q_\chi)$ possesses *three* broad peaks, at around $q_\chi = \pm q_\chi^{\rm EA}$ and $q_\chi = 0$. Such a three-peak structure is rarely seen in a system exhibiting the full RSB, and gives a further indication that the RSB occurring here is the in-field counterpart of the one-step-like RSB.

For $H/J = 0.5$, $P_\chi(q_\chi)$ shows a similar behavior as that for $H/J = 0.05$. Namely, for larger L, it exhibits two distinct peaks, both growing and sharpening with increasing L, whereas it exhibits three broad peaks for an

intermediate L. As compared with the $H/J = 0.05$ case, the second peak is located slightly off $q_\chi = 0$, reflecting the fact that the higher field breaks the $q_\chi \leftrightarrow -q_\chi$ symmetry more strongly. Anyway, our data shown in Figs.8(a)-(c) give a strong numerical support that there indeed occurs a chiral-glass transition at a finite temperature and that the chiral-glass ordered state accompanies a one-step-like RSB.

For the still higher field $H/J = 3.0$, in contrast to the cases of $H/J = 0.05$ and 0.5, the double-peak behavior of $P_\chi(q_\chi)$ is not observed even at the lowest temperature studied $T/J = 0.13$. Thus, for $H/J = 3.0$, no sign of RSB transition is observed down to this low temperature.

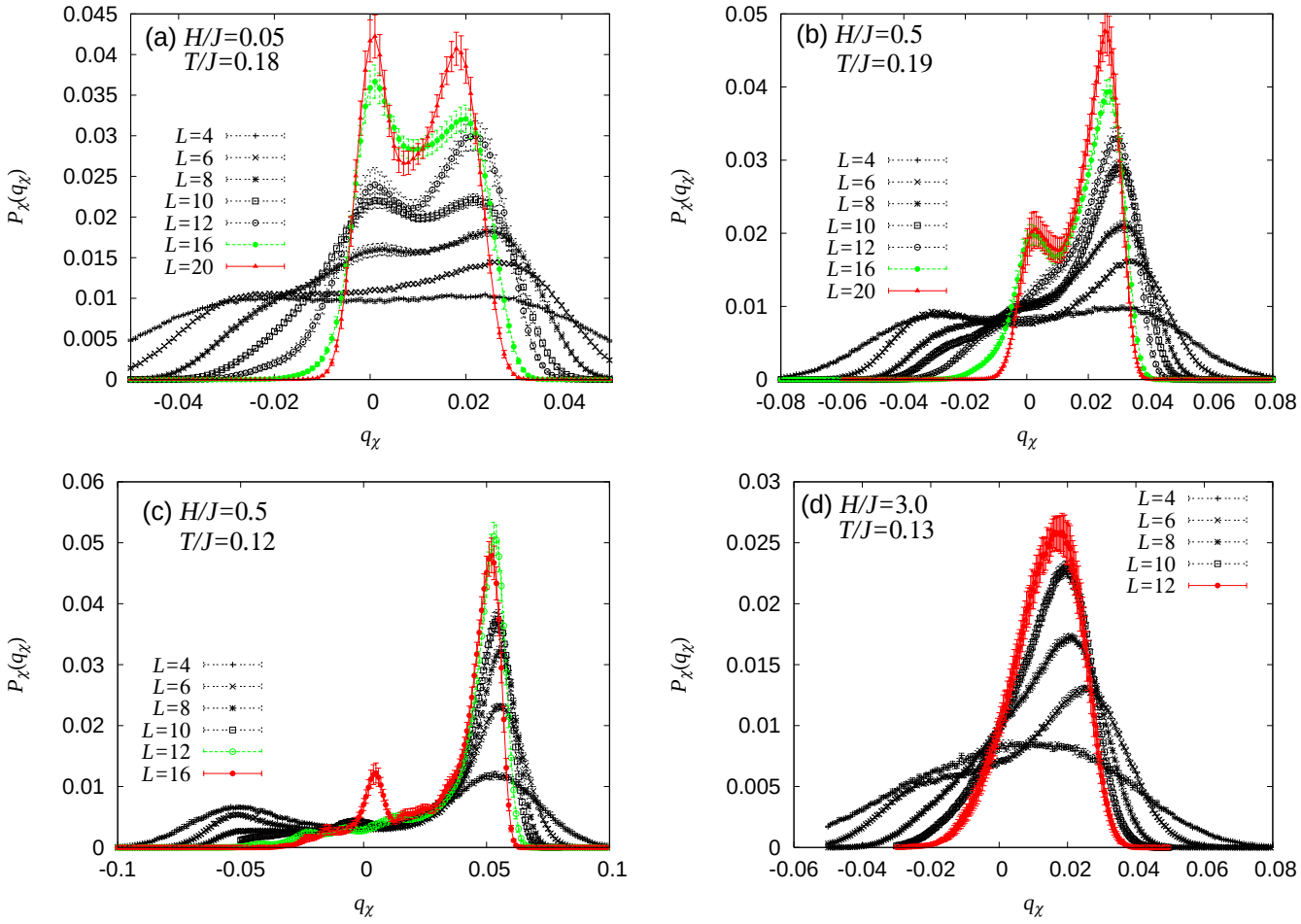

FIG. 8: (Color online) The chiral-overlap distribution functions for the field and the temperature, (a) $H/J = 0.05$ and $T/J = 0.18$, (b) $H/J = 0.5$ and $T/J = 0.19$, (c) $H/J = 0.5$ and $T/J = 0.12$, and (d) $H/J = 3.0$ and $T/J = 0.13$. The transition temperature is $T_g/J \simeq 0.21$ for both cases of $H/J = 0.05$ and 0.5, while it is lower than 0.13 for $H/J = 3$.

G. Overlap distribution function of the spin

We show in Figs.9 the size dependence of the overlap distribution function of (a) the longitudinal component of the spin $P_{\rm s}(q_{\rm L})$, and of (b) the transverse component of the spin $P_{\rm s}(q_{\rm T})$, for the field $H/J = 0.05$ and at a temperature $T/J = 0.18$. The longitudinal spin-overlap distribution function $P_{\rm s}(q_{\rm L})$ for smaller sizes $L \leq 16$ possesses only a single growing peak at around $q_{\rm L} \simeq 0.2$, in apparent contrast to the double-peak structure observed in the chiral-overlap distribution. Quite interestingly, however, for the largest size studied $L = 20$, one sees that the second peak just begins to emerge at around $q_{\rm L} \simeq 0.1$ (see the arrow in Fig.9(a)). This second peak is reminiscent to the one observed in the chiral-overlap distribution function of Fig.8, though it appears here only for the largest size in a less pronounced manner: It appears to be an echo of the strongly diverging $q_\chi \simeq 0$ peak observed in the chiral-overlap distribution. Our observation that the one-step RSB-like structure of

the overlap distribution appears in the chiral sector from smaller sizes, while it appears in the spin sector in a less pronounced manner only for larger sizes, suggests that the order parameter of the present one-step-RSB transition might be the chirality, rather than the spin. Again, this observation is fully consistent with the spin-chirality decoupling-recoupling scenario.[24,25]

As shown in Fig.9(b), the behavior of the transverse-spin-overlap distribution function $P_{\rm s}(q_{\rm T})$ is more complex. Such a behavior is certainly consistent with the occurrence of an RSB transition.

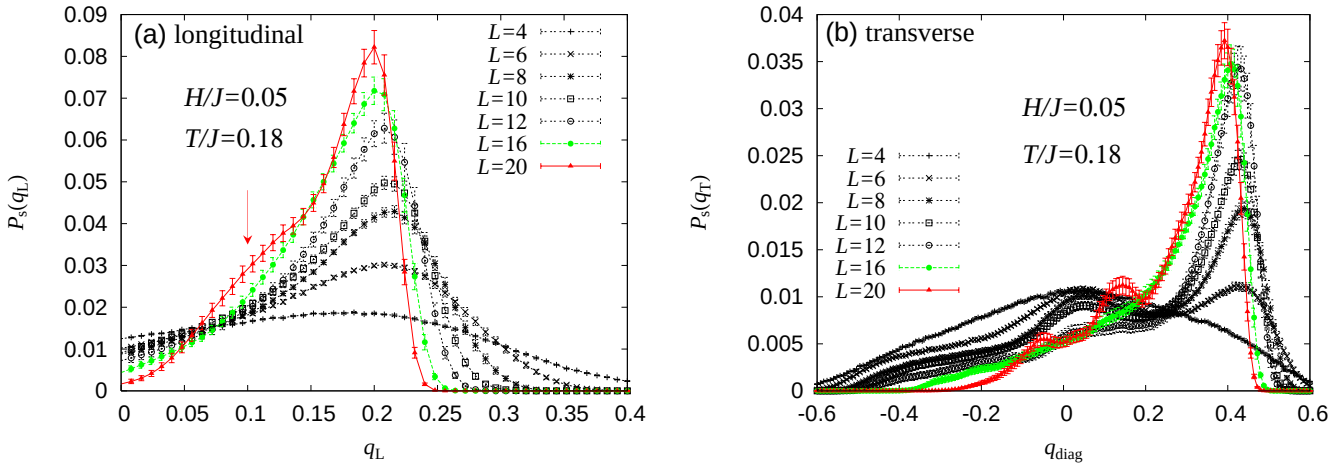

FIG. 9: (Color online) The overlap distribution functions of (a) the longitudinal component of the spin, and of (b) the transverse component of the spin, for a field $H/J = 0.05$ at a temperature $T/J = 0.18$. The transition temperature is $T_g/J \simeq 0.21$. In Fig.(a), a sign of the second peak just begins to emerge for the largest size $L = 20$ at the arrow position.

H. Correlation lengths

We show in Figs.10 the temperature and size dependence of the normalized correlation lengths of (a) the chirality ξ_χ/L, of (b) the longitudinal component of the spin $\xi_{\rm L}/L$, and of (c) the transverse component of the spin $\xi_{\rm T}/L$, for the field $H/J = 0.05$. The location of $T_g(H)$ obtained from the autocorrelation functions are displayed with arrows in the figures.

Concerning the chirality, as can be seen from the inset of Fig.10(a). a clear crossing behavior is observed at $T/J \simeq 0.22$ for larger sizes $L \geq 12$. The crossing temperature $T/J \simeq 0.21$ observed for larger sizes turns out to be close to our previous estimate of T_g.

Concerning the longitudinal and the transverse components of the spin, a crossing is observed at $T_g/J \simeq 0.21$ for smaller sizes $L \leq 8$. For $L \geq 10$, however, ξ/L decreases with L at any temperature studied, no longer exhibiting a crossing at $T_g/J \simeq 0.21$. For even larger sizes $L = 16$ and $L = 20$, a tendency of crossing re-appears at around $T_g/J \simeq 0.21$, but now at a lower value of ξ/L.

Such a complex size dependence of the spin correlation lengths may naturally be interpreted by the spin-chirality decoupling-recoupling scenario in the following way: For smaller sizes, *i.e.*, at shorter length scales, the spin and the chirality are trivially coupled in correlations irrespective of the anisotropy, so that the crossing in the sizes $L \leq 8$ may reflect this trivial coupling at short length scales. For larger sizes, *i.e.*, at long length scales, the spin is "recoupled" to the chirality via the anisotropy in a way different from the trivial coupling at short length scales. Thus, the two different types of crossing is expected in the normalized correlation lengths for smaller and for larger sizes, which is exactly the behavior observed in Figs.10(b) and (c). The characteristic length scale separating the coupling and the recoupling regimes was estimated to be about 20 lattice spacings.[29,38] Therefore, although we cannot simulate here the sizes larger than $L = 20$ due to the lack of our computational capability, we do expect that a clear crossing behavior will eventually set in for $L > 20$.

V. THE CRITICAL PROPERTIES AND THE PHASE DIAGRAM

In this section, we further analyze the nature of the chiral-glass (spin-glass) transition observed in the previous section by means of a scaling analysis, and construct a magnetic phase diagram of the model in the temperature

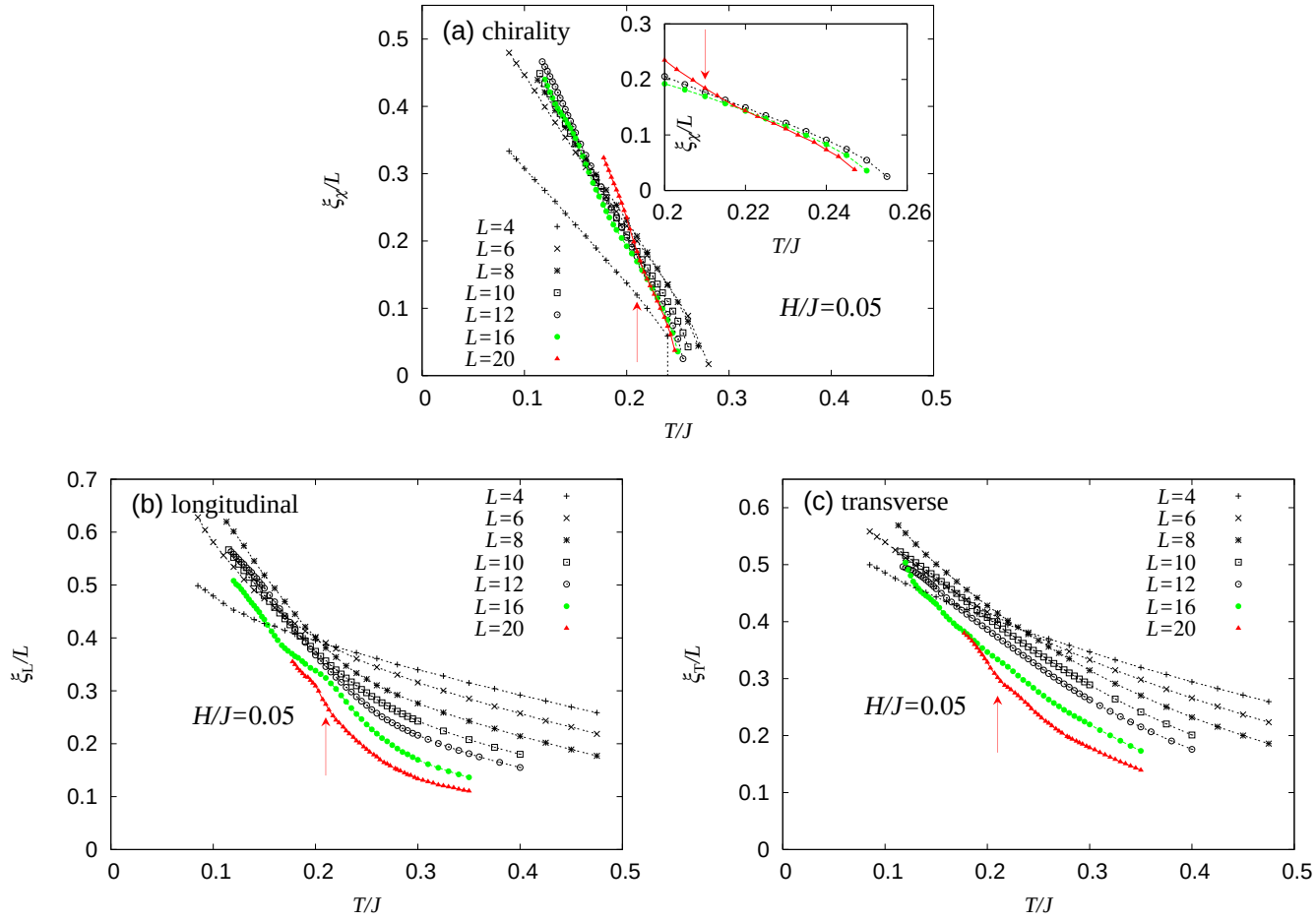

FIG. 10: (Color online) The temperature and size dependence of the normalized correlation lengths of (a) the chirality, of (b) the longitudinal component of the spin, and of (c) the transverse component of the spin, for a field $H/J = 0.05$. In Fig.(a), a magnified figure is given in the inset for the three largest sizes, $L = 12$, 16 and 20. The arrows in the figures indicate the locations of $T_g(H)$, *i.e.*, $T_g/J = 0.21$.

- magnetic field plane.

We apply a dynamical scaling analysis to the chiral autocorrelation functions in order to estimate the critical exponents of the transition. The standard bulk dynamical scaling form is assumed for the autocorrelation functions, $\tilde{C}_\chi(t)$, $\tilde{C}_{\rm L}(t)$ and $\tilde{C}_{\rm T}(t)$,

$$\tilde{C}(t) \approx |(T - T_g)/J|^\beta f(t|(T - T_g)/J|^{z\nu}) \tag{32}$$

where T_g is the transition temperature determined in the previous section, while β, ν and z refer to the order parameter, the correlation-length and the dynamical exponents, respectively. The exponents β and $z\nu$ are to be determined so that a good data collapse is obtained in the scaling plot. The quality of the scaling plot is judged by eyes.

A. Dynamical scaling analysis of the chiral autocorrelation function

In Figs.11, we show the scaling plots of the chiral autocorrelation function $\tilde{C}_\chi(t)$ for the fields (a) $H/J = 0.05$ and (b) $H/J = 0.5$. The transition temperature is fixed to be $T_{\rm CG}/J = 0.21$ both for $H/J = 0.05$ and $H/J = 0.5$, as determined in the previous section.

As can be seen from the figures, the chiral autocorrelation function scales well both above and below T_g, with $\beta_{\rm CG} = 0.8$ and $z_{\rm CG}\nu_{\rm CG} = 5.0$ for $H/J = 0.05$, and with $\beta_{\rm CG} = 0.7$ and $z_{\rm CG}\nu_{\rm CG} = 5.5$ for $H/J = 0.5$. Examining by eyes the quality of the scaling plots with varying the assumed exponents values, we finally quote $\beta_{\rm CG} = 0.8 \pm 0.2$

and $z_{\rm CG}\nu_{\rm CG} = 5.0\pm1.0$ for $H/J = 0.05$, and $\beta_{\rm CG} = 0.7\pm0.2$ and $z_{\rm CG}\nu_{\rm CG} = 5.5\pm1.0$ for $H/J = 0.5$. The estimated chiral-glass exponents are not far from the corresponding zero-field values $\beta_{\rm CG} \simeq 1.1$[25] and $z_{\rm CG}\nu_{\rm CG} \simeq 4.5$.[28]

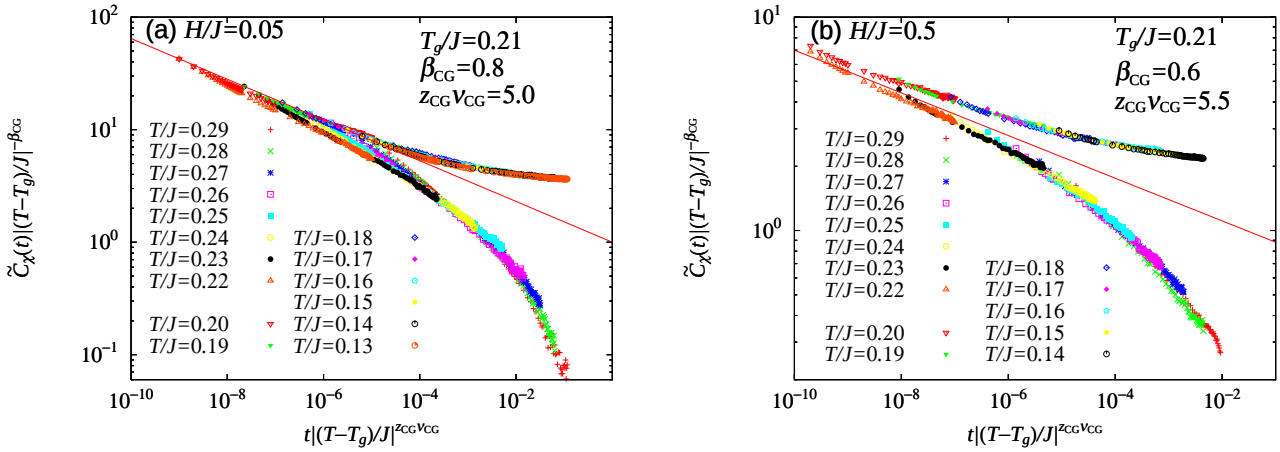

FIG. 11: (Color online) Dynamical scaling plots of the chiral autocorrelation function $\tilde{C}_\chi(t)$, for fields (a) $H/J = 0.05$ and (b) $H/J = 0.5$.

B. Dynamical scaling analysis of the spin autocorrelation functions

Next, we apply a dynamical scaling analysis to the spin autocorrelation functions. In Figs.12, we show the scaling plots both for (a) the longitudinal and for (b) the transverse components of the spin for the field $H/J = 0.05$. The transition temperature is fixed to be $T_g/J = 0.21$. In Ref.[32], we observed that the quality of the scaling plot of the spin time-correlation function $q_{\rm L}^{(2)}$ was not as good as its chiral counterpart $q_\chi^{(2)}$. As argued in Ref.[32], if the chirality, rather than the spin, is the order parameter of the transition, in the time regime shorter than the recoupling time scale (estimated to be $10^5 \sim 10^6$ MCS), the spin time-correlation might not reach an asymptotic scaling regime even when the chiral time-correlation reaches an asymptotic scaling regime. Hence, although the scaling of $\tilde{C}_{\rm L}(t)$ and $\tilde{C}_{\rm T}(t)$ turns out to be fairly good as shown in Fig.12, caution might be required here in regarding the fitted values of $\beta_{\rm SG}$ and $z_{\rm SG}\nu_{\rm SG}$ as true asymptotic spin exponents, since our observation time window is shorter than the expected recoupling time scale.

C. Chiral-glass and spin-glass susceptibilities

In order to estimate the chiral-glass and the spin-glass susceptibility exponents $\gamma_{\rm CG}$ and $\gamma_{\rm SG}$, we plot in Figs.13 (a) the reduced chiral-glass susceptibility $\tilde{\chi}_\chi$, and (b) the transverse spin-glass susceptibility $\tilde{\chi}_{\rm T}$, as a function of the reduced temperature $(T-T_g)/T_g$ for the field $H/J = 0.05$ on a log-log plot. The chiral-glass and the spin-glass susceptibilities in the thermodynamic limit are expected to behave as

$$\tilde{\chi}_\chi \approx |T - T_g|^{-\gamma_{\rm CG}}, \qquad \tilde{\chi}_{\rm T} \approx |T - T_g|^{-\gamma_{\rm SG}}. \tag{33}$$

The T_g value is fixed to be $T_g/J = 0.21$. From the asymptotic slope of the data, the exponents $\gamma_{\rm CG}$ and $\gamma_{\rm SG}$ are estimated to be $\gamma_{\rm CG} = 2.1(2)$ and $\gamma_{\rm SG} = 2.4(2)$, respectively. Here, the obtained values of $\gamma_{\rm SG}$ and $\gamma_{\rm CG}$ turn out to be rather close. Indeed, the spin-chirality decoupling-recoupling scenario predicts an equality $\gamma_{\rm SG} = \gamma_{\rm CG}$.

D. H-T phase diagram

Finally, we show in Fig.14 a phase diagram of the present model with $D/J = 0.05$ in the temperature-magnetic field plane. The obtained phase diagram has two noticeable features. First, for weaker fields $H/J \lesssim 0.05 = D/J$, the transition line $T_g(H)$ exhibits an AT-like like behavior, *i.e.*, the spin-glass (chiral-glass) transition temperature

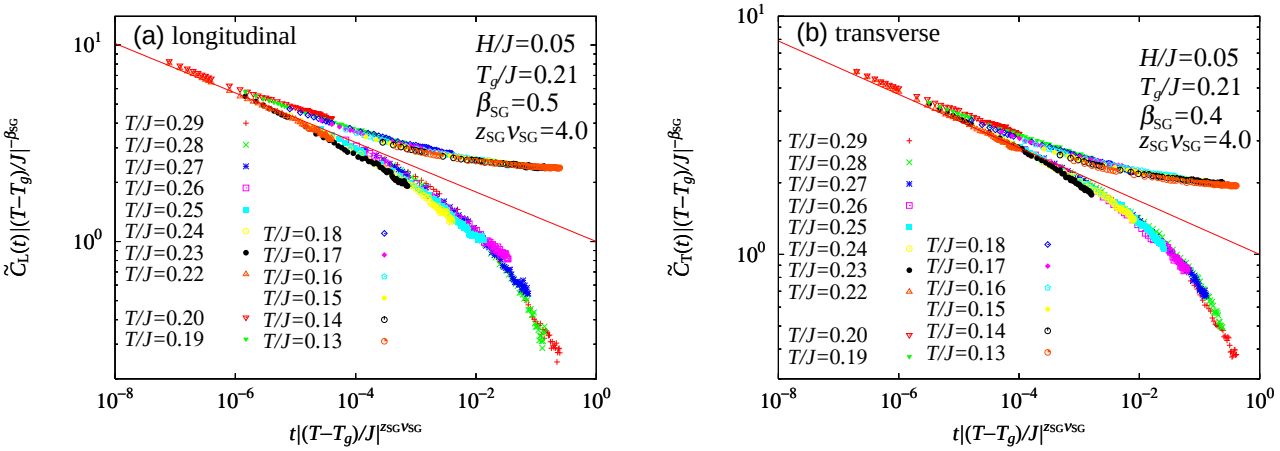

FIG. 12: (Color online) Dynamical scaling plots of the autocorrelation functions of (a) the longitudinal component of the spin $\tilde{C}_{\rm L}$, and of (b) the transverse component of the spin $\tilde{C}_{\rm L}$, for a field $H/J = 0.05$.

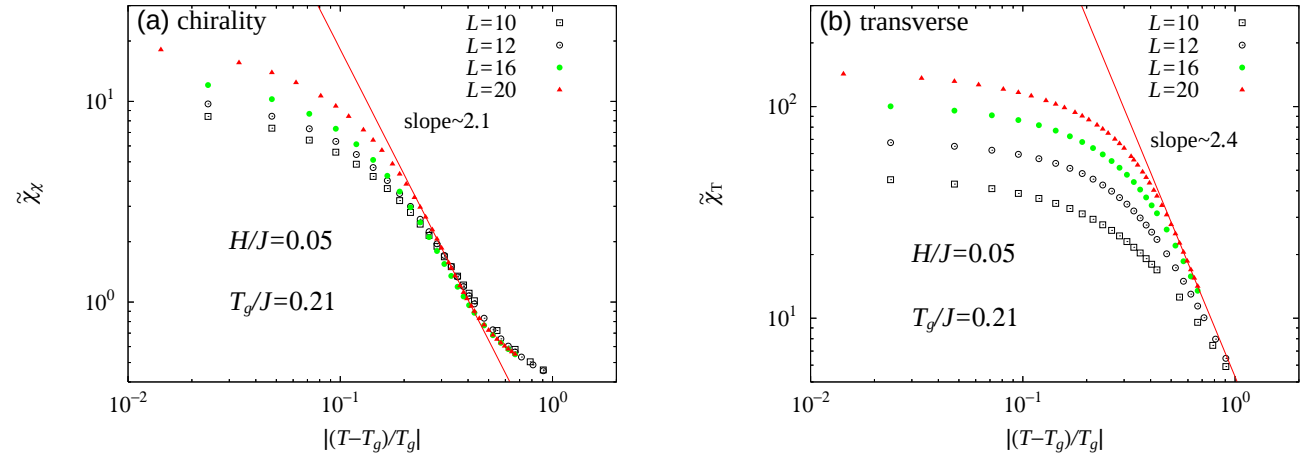

FIG. 13: (Color online) Temperature and size dependence of (a) the chiral-glass susceptibility, and of (b) the transverse spin-glass susceptibility, for a field $H/J = 0.05$. The transition temperatures is set to be $T_g/J = 0.21$.

is suppressed rapidly under weak applied fields. In sharp contrast to this, for stronger fields of $H/J \gtrsim 0.05 = D/J$, the spin-glass (chiral-glass) transition temperature turns out to be rather insensitive to the field intensity, indicating that the spin-glass (chiral-glass) ordered state is robust against applied fields. The estimated $T_g(H)$ value stays almost unchanged between the field values $H/J = 0.05$ and 0.5, the latter value is already more than twice the zero-field transition temperature. Indeed, the $T_g(H)$ value in this field range is very close to the zero-field chiral-glass transition temperature of the fully *isotropic* model. This is exactly the feature of the GT line.

Overall, the obtained phase diagram is consistent with the experimental phase diagram of Heisenberg-like SG magnets.[1,3,4] In order to make a more quantitative comparison, however, we have to determine the phase boundary in the lower field regime $H/J \leq 0.05$ more precisely, and to map out a phase diagram with varying the anisotropy strength D. This is a computationally demanding task, and is left as a future task.

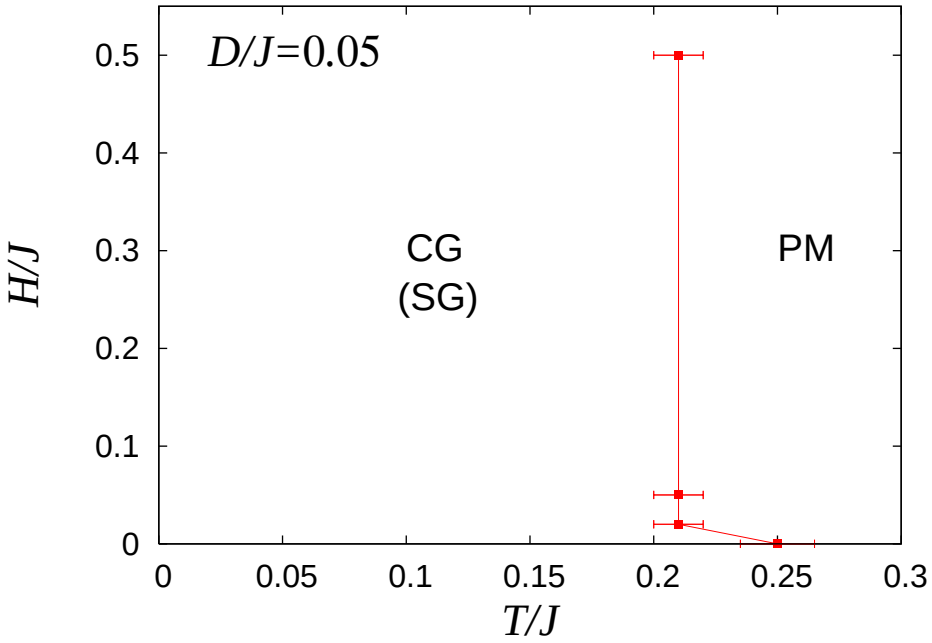

FIG. 14: (Color online) The phase diagram of the anisotropic Heisenberg SG with the random anisotropy of $D/J = 0.05$ in the temperature-magnetic field plane. "CG", "SG" and "PM" stand for the "chiral-glass", "spin-glass" and "paramagnetic" phase, respectively.

VI. SUMMARY AND DISCUSSION

In summary, we performed a large-scale equilibrium Monte Carlo simulation of the weakly anisotropic 3D Heisenberg SG in magnetic fields, paying attention both to the spin and to the chirality. The model is expected to be a reasonably realistic model of many real Heisenberg-like SG magnets. Due to the presence of both the random anisotropy and the magnetic field, the model lacks in any global symmetry so that the transition, if any, is expected to be a pure RSB one. Among other things, we have found a clear numerical evidence that such a pure RSB transition indeed occurs at a finite temperature simultaneously in the spin and in the chiral sectors. The temporal decay of the time correlation functions of the chirality and of the spin, as well as the overlap distribution function of the chirality and the spin, gave a strong numerical evidence of the occurrence of a thermodynamic RSB transition in applied fields. We feel this finding for the weakly anisotropic Heisenberg SG to be rather remarkable, in view of the long controversy in the community concerning the in-field ordering properties of the Ising SG, which apparently looks much simpler.

Indeed, a comparison with the 3D Ising SG in fields have revealed that the weakly anisotropic Heisenberg SG in fields behaves differently from the Ising SG in fields, a sign of the RSB transition being much clearer in the weakly anisotropic Heisenberg SG than in the Ising SG. The observed stronger sign of the RSB transition is closely connected to the one-step-like nature of its RSB pattern, which is certainly not the case in the Ising SG. Such a difference in the ordering properties of the two models might at first sound surprising, since the Ising SG in fields and the weakly anisotropic Heisenberg SG in fields share the same symmetry property. However, in spite of the similarity in symmetry, a significant difference exists in the two models in that the Ising SG does not possess any chirality degree of freedom in contrast to the weakly anisotropic Heisenberg SG. Then, our observation highlights the possible importance of the chirality in realizing the RSB transition in the weakly anisotropic Heisenberg SG. This gives a strong support to the chirality scenario of the SG transition of Heisenberg-like SGs.[24,25]

We also have found that the sign of the RSB transition is often observed more strongly in the chirality-related quantities than in the spin-related quantities. For example, the second peak of the overlap distribution function shows up clearly even from smaller lattices for the chirality, but more weakly and only for larger lattices for the spin: Compare Fig.8(a) and Fig.9(a). This observation seems consistent with the chirality scenario that the order parameter of the transition is the chirality whereas the spin is recoupled to the chirality beyond a certain crossover (recoupling) length scale of about 20 lattice spacings. We have also observed that the behaviors of certain spin-related quantities, *e.g.*, the Binder ratio or the normalized correlation length, differ between in smaller and in larger lattices, the borderline size being around $L \simeq 20$. Again, these behaviors could naturally be explicable on

the basis of the spin-chirality decoupling-recoupling scenario.[24,25]

We also have constructed a rough H-T phase diagram of the model. It has turned out that $T_g(H)$ is rapidly suppressed by weak applied fields, $H \lesssim D$, but is then kept almost unchanged up to rather higher fields of $H/J = 0.5 \approx 2T_g(0)$. The phase boundary in the weak field regime resembles the AT-line, while that in the high field regime resembles the GT line, although its nature is very different from the mean-field AT- or GT-line.[5,6,7] These features of the phase diagram are consistent with the experimental result of the weakly anisotropic Heisenberg SG.[3,4] The obtained phase diagram is also fully consistent with the one expected from the chirality scenario.[24,25,30,32] Indeed, the chirality scenario predicts that, in the low-field regime where the anisotropy is important, the change in the broken symmetry from the zero-field case causes a crossover, accompanied with a rapid suppression of the transition temperature, while in the high-field regime where the anisotropy is negligible relative to the applied magnetic field, the SG transition line should essentially be given by the chiral-glass transition line of the fully isotropic system.[30]

Another remarkable feature of the present phase diagram is that the GT-like phase boundary is quite robust against magnetic fields, extending without much reduction to the field at least as twice large as the zero-field transition temperature. Such a robustness of the SG ordered phase under fields is also in accord with the chirality scenario, since the chirality, regarded as a hidden order parameter of the SG transition, is only weakly coupled to the magnetic field. Note that the magnetic field couples directly to the spin via the Zeeman term in the Hamiltonian, not to the chirality, while the effective coupling between the field and the chirality is rather weak.

Thus, overall, our observations on the weakly anisotropic Heisenberg SG gives a strong support to the spin-chirality decoupling-recoupling scenario.[24,25] In other words, it would be difficult to interpret all of our present observations based on the more conventional view that the spin is the order parameter of the transition and the chirality is just a composite (secondary).

A decisive test of the spin-chirality decoupling-recouping scenario would be to directly probe the chiral-glass order. Recently, a proposal was made concerning the way to measure the linear and the nonlinear chiral susceptibilities of canonical SGs by using the Hall probe, together with the scaling prediction from the spin-chirality decoupling-recoupling scenario.[42,43] Interestingly, very recent experiments have given support to these predictions from the chirality scenario.[44,45,46]

In concluding this paper, we wish to emphasize again that, even if one sets aside the question of the detailed mechanism of the SG transition or the validity of the chirality scenario, the present numerical results have demonstrated beyond reasonable doubt that the weakly anisotropic Heisenberg SG exhibits a thermodynamic RSB transition in applied magnetic fields. In view of the fact that the property of the apparently simpler, strongly anisotropic Ising SG still remains unclear in spite of the long controversy, this finding seems surprising and somewhat ironical. Clarifying the relation between the weakly anisotropic Heisenberg SG possessing the chiral degree of freedom and the strongly anisotropic Ising SG not possessing the chiral degree of freedom is still open, and is left for future studies.

Acknowledgments

The numerical calculation was performed on the HITACHI SR8000 at the supercomputer system, ISSP, University of Tokyo, and Pentium IV clustering machines in our laboratory. The authors are thankful to I.A. Campbell, K. Hukushima, H. Yoshino, and G. Tatara for useful discussion and comments.

[1] For reviews on spin glasses, see *e. g.,* K. Binder and A. P. Young, Rev. Mod. Phys. **58** 801 (1986); K. H. Fischer and J. A. Hertz, *Spin Glasses* (Cambridge University Press, Cambridge, 1991); J. A. Mydosh: *Spin Glasses*, (Taylor & Francis, London·Washington DC, 1993); *Spin glasses and random fields*, *ed.* A. P. Young (World Scientific, Singapore, 1997).
[2] J. Mattsson, T. Jonsson, P. Nordblad, H. ArugaKatori and A. Ito, Phys. Rev. Lett. **74**, 4305 (1995).
[3] D. Petit, L. Fruchter and I. A. Campbell, Phys. Rev. Lett. **83**, 5130 (1999).
[4] D. Petit, L. Fruchter, and I. A. Campbell Phys. Rev. Lett. **88**, 207106 (2002).
[5] G. Kotliar and H. Sompolinsky, Phys. Rev. Lett. **53**, 1751 (1984).
[6] J. R. L. de Almeida and D. J. Thouless, J. Phys. A **11**, 983 (1978).
[7] M. Gabay and G. Toulouse, Phys. Rev. Lett. **47**, 201 (1981).
[8] E. R. Grannan and R. E. Hetzel, Phys. Rev. Lett. **67**, 907 (1991).
[9] R. R. P. Singh and D. A. Huse, J. Appl. Phys. **69**, 5225 (1991).
[10] N. Kawashima, N. Ito and M. Suziki, J. Phys. Soc. Jpn. **61**, 1777 (1992); N. Kawashima and N. Ito, *ibid* **62**, 435 (1993).
[11] D. Badoni, J.C. Ciria, G. Parisi, F. Ritort, J. Pech and J.J. Ruiz-Lorezo, Europhys. Letters **21**, 495 (1993).
[12] E. Marinari, G. Parisi and F. Zuliani, J. Phys. A **31**, 1181 (1998).
[13] M. Picco and F. Ritort, Physica A **250**, 46 (1998).

[14] G. Parisi, F. Ricci-Tersenghi and J. J. Ruiz-Lorenzo, Phys. Rev. B **57**, 13617 (1998).
[15] J. Houdayer and O.C. Martin, Phys. Rev. Lett **82**, 4934 (1999); E. Marinari, G. Parisi and F. Zuliani, *ibid*, **84**, 1056 (2000); J. Houdayer and O.C. Martin, *ibid*, **84**, 1057 (2000).
[16] F. Krzakala, J. Houdayer, E. Marinari, O.C. Martin and G. Parisi, Phys. Rev. Lett. **87**, 197204 (2001).
[17] J. Lamarcq, J.-P. Bouchaud and O.C. Martin, Phys. Rev. B **68**, 012404 (2003).
[18] A. Cruz, L. A. Fernández, S. Jiménez, J. J. Ruiz-Lorenzo and A. Tarancón, Phys. Rev. B **67**, 214425 (2003).
[19] J. R. Banavar and M. Cieplak, Phys. Rev. Lett. **48**, 832 (1982); M. Cieplak and J. R. Banavar, Phys. Rev. B **29**, 469 (1984).
[20] W. L. McMillan, Phys. Rev. B **31**, 342 (1985).
[21] J. A. Olive and A. P. Young and D. Sherrington, Phys. Rev. B **34**, 6341 (1986).
[22] F. Matsubara and T. Iyota and S. Inawashiro, Phys. Rev. Lett. **67**, 1458 (1991).
[23] H. Yoshino and H. Takayama, Europhys. Lett. **22**, 631 (1993).
[24] H. Kawamura, Phys. Rev. Lett. **68**, 3785 (1992); Int. J. Mod. Phys. C **7**, 6341 (1996).
[25] H. Kawamura, Phys. Rev. Lett. **80**, 5421 (1998).
[26] H. Kawamura, J. Phys. Soc. Jpn. **64**, 26 (1995).
[27] K. Hukushima and H. Kawamura, Phys. Rev. E **61**, R1008 (2000).
[28] M. Matsumoto, K. Hukushima and H. Takayama, Phys. Rev. B **66**, 104404 (2002).
[29] K. Hukushima and H. Kawamura, to be published; H. Kawamura and K. Hukushima, Activity Report of ISSP Supercomputer Center 2002, 11 (2003).
[30] H. Kawamura and D. Imagawa, Phys. Rev. Lett. **87**, 207203 (2001).
[31] D. Imagawa and H. Kawamura, J. Phys. Soc. Jpn. **71**, 127 (2002).
[32] D. Imagawa and H. Kawamura, Phys. Rev. Lett. **92**, 077204 (2004).
[33] F. Matsubara and S. Endoh and T. Shirakura, J. Phys. Soc. Jpn. **69**, 1927 (2000); S. Endoh, F. Matsubara and T. Shirakura, J. Phys. Soc. Jpn. **70**, 1543 (2001); F. Matsubara, T. Shirakura and S. Endoh, Phys. Rev. B **64**, 092412 (2001).
[34] T. Nakamura and S. Endoh, J. Phys. Soc. Jpn. **71**, 2113 (2002).
[35] L. W. Lee and A. P. Young, Phys. Rev. Lett. **90**, 227203 (2003).
[36] L. Berthier and A. P. Young, cond-mat/0312327.
[37] K. Hukushima and K. Nemoto, J. Phys. Soc. Jpn. **65**, 1604 (1995).
[38] H. Kawamura and M.S. Li, Phys. Rev. Lett. **87**, 187204 (2001).
[39] D. Imagawa and H. Kawamura, Phys. Rev. B **67**, 224412 (2003).
[40] K. Hukushima and H. Kawamura, Phys. Rev. E **62**, 3360 (2000).
[41] M. Picco, F. Ritort and M. Sales, Eur. Phys. J. B **19**, 565 (2001).
[42] G. Tatara and H. Kawamura, J. Phys. Soc. Jpn. **71**, 2613 (2002).
[43] H. Kawamura, Phys. Rev. Lett. **90**, 047202 (2003).
[44] T. Taniguchi, K. Yamanaka, H. Sumioka, T. Yamazaki, Y. Tabata and S. Kawarazaki, submitted.
[45] P. Pureur, F. Wol Fabris, J. Schaf and I. A. Campbell, Europhys. Lett. in press, cond-mat/0312311.
[46] N. Aito, M. Soda, Y. Kobayashi and M. Sato, J. Phys. Soc. Jpn. **72**, 1226 (2003); T. Kageyama, N. Aito, S. Iikubo and M. Sato, J. Phys. Soc. Jpn. **72**, 1491 (2003).